Indonesian Physical Review

Impact of Zn-Dopped on SNEDDS/$Zn_xFe_{3-x}O_4$ Formulation on Their Crystal Structure and Antioxidant Performance

Uvia Ardina Zahira[1], Nadiya Miftachul Chusna[1,2], Ahmad Taufiq[1,3], Sunaryono Sunaryono[1,3,*]

[1] Department of Physics, Faculty of Mathematics and Natural Sciences, Universitas Negeri Malang, Indonesia.
[2] Mions Laboratory, PT Cakra Mions Teknologi (Persero, Indonesia.
[3] PUI-Centre of Advanced Materials for Renewable Energy (CAMRY), Universitas Negeri Malang, Indonesia.

Corresponding Authors E-mail: sunaryono.fmipa@um.ac.id

Article Info

Abstract

Self-Nano-Emulsifying Drug Delivery System (SNEDDS)/$Zn_xFe_{3-x}O_4$ has been successfully formulated through the synthesis of $Zn_xFe_{3-x}O_4$ by the coprecipitation method and SNEDDS/$Zn_xFe_{3-x}O_4$ by the sonication method. This study is focused on the effect of Zn doping on the crystal structure and antioxidant performance of $Zn_xFe_{3-x}O_4$ nanoparticles. $Zn_xFe_{3-x}O_4$ samples were characterized using FTIR and XRD to determine the functional groups and structure of the sample, respectively. SNEDDS/$Zn_xFe_{3-x}O_4$ samples were characterized using FTIR and Antioxidants with the DPPH method to determine the functional groups and antioxidants in the sample, respectively. The FTIR characterization results of the $Zn_xFe_{3-x}O_4$ sample showed the emergence of Zn-O and Fe-O functional groups in the wave number range of 825-869 cm^{-1} and 560-594 cm^{-1}, respectively. This indicates that Zn^{2+} doping was successfully synthesized and shifted the Fe^{3+} ion. The IR spectrum also shows that the higher the concentration of Zn^{2+} ions, the more significant the change in absorption intensity, indicating that more molecules absorb light at wave numbers of 825-869 cm^{-1}. The XRD characterization results show that the $Zn_xFe_{3-x}O_4$ nanoparticle structure is an inverse cubic spinel occupying the Fd3m crystal group. Based on the analysis of XRD data, the higher the concentration of Zn^{2+} doping, the smaller the size of the $Zn_xFe_{3-x}O_4$ nanoparticles produced. The diffraction peak of the sample on the 311 plane shifts towards a smaller angle due to the effectiveness of Zn^{2+} ion doping, shifting the Fe^{3+} ion because the radius of the Zn^{2+} ion is larger than the Fe^{3+} one. The antioxidant performance analysis of SNEDDS/ZnxFe3-xO4 showed inhibition potential ranging from 11% to 15%, increasing with higher Zn^{2+} concentrations.

Introduction

Antioxidant agents are very important for the body. Antioxidants in the body are an effort to inhibit the production of free radicals in human body metabolism [1]. Free radicals have a

significant influence on inflammation, ageing, and causes of cancer [2]. On the other hand, antioxidants can also prevent disease development [1], so antioxidants have become essential in the medical field, including the drug delivery system (DDS). DDS with good antioxidant performance can minimize the side effects of drugs in the body [3].

Research on various drug delivery systems is currently significantly developed and in great demand. One of them is the Self Nano Emulsifying Drug Delivery System (SNEDDS), which can form emulsions spontaneously when in the digestive tract [4]. SNEDDS consists of oil, surfactants, and cosurfactants [5], which generally have their respective roles. Oil is a carrier of drugs or active substances in SNEDDS [6]. Surfactants act as emulsifiers in the nano order and prevent drug sedimentation in the digestive tract. Cosurfactants play a role in improving the dispersibility and absorption of active substances in the body [7].

Based on its function, SNEDDS has several advantages. One of the advantages of SNEDDS is its small particle size (below 200 nm), which maximizes the absorption of drugs or active substances in SNEEDS due to its high surface area [8]. However, as a drug delivery system, SNEDDS cannot be directed or controlled towards the target [9]. From several research developments, SNEDDS can be combined with magnetite nanoparticles, namely Fe_3O_4, so that the drug delivery system can be appropriately directed according to the desired target [10]. Fe_3O_4 nanoparticles have good biocompatibility and low toxicity to the human body [11]. In addition, Fe_3O_4 nanoparticles in bulk form have ferrimagnetic properties, and in nanoscale below 14 nm, they may have superparamagnetic properties [12], which can be used as basic materials in drug delivery systems. The superparamagnetic properties of Fe_3O_4 nanoparticles indicate that the magnetization of the particles can be close to zero if there is no magnetic field and has a magnetization almost the same as the magnetic field given to it [13]. This helps direct the drug precisely to the target for release. This directed drug delivery using magnetic fields will reduce the side effects of medications given to patients [14]. In addition, Fe_3O_4 nanoparticles also have excellent antioxidant performance. Based on research by Anigol et al. [15] iron nanoparticles showed good antioxidant activity against DPPH with a percentage of 85%.

Several other studies have reported on adding Zn doping to Fe_3O_4 nanoparticles. One is a study conducted by Priyanka Saha et al. [16]. This study successfully synthesized $Zn_xFe_{3-x}O_4$ and studied the magnetization dynamics of Zn doping. The energy interaction between particles decreased with increasing Zn doping. However, this study did not specifically discuss the antioxidant potential of the sample. Research by Ping Hou et al. [17] successfully synthesized Fe_3O_4@starch/Cu nanocomposites and investigated their antioxidant performance using the DPPH method. The antioxidant inhibition of Fe_3O_4@starch/Cu nanocomposites gradually increased with increasing sample concentration.

Meanwhile, in the study of Usman et al. [18], the Zn^{2+} ion medium successfully increased the antioxidants of natural materials by increasing the blanching process in $ZnCl_2$ and Zn acetate. From several previously reported studies, there are still few studies that combine SNEDDS material with Fe_3O_4 nanoparticles. Several studies have reported SNEDDS with plant extracts. Therefore, it is necessary to formulate SNEDDS/$Zn_xFe_{3-x}O_4$ with variations in the addition of Zn doping. It is essential to know the effectiveness of the sample as an antioxidant from the SNEDDS formulation that can be directed. SNEDDS formulations must contain antioxidants to protect the drug and reduce side effects. The novelty of this research is that it formulates SNEDDS with $Zn_xFe_{3-x}O_4$ as a potential antioxidant in SNEDDS that can be directed directly

at the drug target. This research focused on the high antioxidant potential of the basic formulation of SNEDDS. However, it must have good magnetic properties for targeted drug delivery. This report presents a comprehensive study of the crystal structure due to the influence of Zn doping.

Experimental Method

Materials

Iron sand is the main material used to provide Fe^{2+} and Fe^{3+} ions. The sand was obtained from Sine Beach Tulungagung, Indonesia. The reduction used is hydrogen chloride (HCl) 12 M, 99,9% (Merck Germany), ammonium hydroxide (NH_4OH) 6,5 M, 99,9% (Merck Germany). The main ingredients of SNEDDS use surfactants Tween 80 (Merck Germany), cosurfactants Polyethene Glycol (PEG) 400 (Sigma Aldrich) and oil pure VCO, and Zinc Chloride ($ZnCl_2$) (Merck Germany), ethanol, and distilled water.

Synthesis of $Zn_xFe_{3-x}O_4$ Nanoparticles

The synthesis of $Zn_xFe_{3-x}O_4$ nanoparticles began with separating iron sand using a permanent magnet to separate the pure iron sand with silica sand, 20 grams of iron sand from the separation with 58 ml of HCl solution. The mixture was stirred on a magnetic stirrer hotplate for 30 minutes at a speed of 720 rpm at room temperature between 22-30℃. Furthermore, the mixture was filtered to produce $FeCl_2$ and $FeCl_3$ solutions following equation (1). 18 mL of $FeCl_2$ and $FeCl_3$ solutions were then stirred on a magnetic stirrer hotplate for 10 minutes at a speed of 720 rpm at room temperature, then adding 1.090 g of $ZnCl_2$. This step was repeated 3 times for different x variations, namely 0, 0.5, 1, and 1.5, each containing a mass of 0, 1.090, 2.137, and 3.143 grams (sample names and sample codes are presented in Table 1). The mixture was then titrated with 25 ml of NH_4OH solution using a dropping pipette and stirred on a magnetic stirrer hotplate for 10 minutes. The mixture was then washed using distilled water until pH 7. The washed mixture was dried using a microwave for 1 hour at 100 °C. Finally, the mixture was ground using a mortar to become $Zn_xFe_{3-x}O_4$ powder.

$$Fe_3O_4 + 8HCl \rightarrow 2FeCl_3 + FeCl_2 + 4H_2O \tag{1}$$

Table 1. Sample names and sample codes of $Zn_xFe_{3-x}O_4$ nanoparticles.

Sample Name	Sample Code
Fe_3O_4	X0
$Zn_{0.5}Fe_{2.5}O_4$	X1
$ZnFe_2O_4$	X2
$Zn_{1.5}Fe_{1.5}O_4$	X3

Formulations of SNEDDS/$Zn_xFe_{3-x}O_4$ Ferrofluid

The synthesis process of SNEDDS/$Zn_xFe_{3-x}O_4$ ferrofluid begins by mixing Tween 80 and PEG 400 with a ratio of mass 3:1 and stirring using a hotplate magnetic stirrer at a speed of 720 rpm for 10 minutes at room temperature between 22-30℃ and left for 24 hours which is then referred to as mixture A. On the other hand, 0.012 g of sample X0 was added with 5 ml of ethanol Pa and then sonicated for 90 minutes, which is then referred to as mixture B. This process was repeated 3 times for samples X1, X2, and X3. The next step is to composite mixtures A and B followed by the addition of VCO with a mixture and VCO ratio of mass 9:1. The mixture is then stirred on a hotplate magnetic stirrer for 20 minutes at room temperature between 22-30 ℃ and continued with sonication for 90 minutes. Figure An illustrates the

$SNEDDS/Zn_xFe_{3-x}O_4$ ferrofluid synthesis method, as shown in Figure 1 and the sample coding in Table 2.

Table 2. Sample names and sample codes of $SNEDDS/Zn_xFe_{3-x}O_4$ nanoparticles.

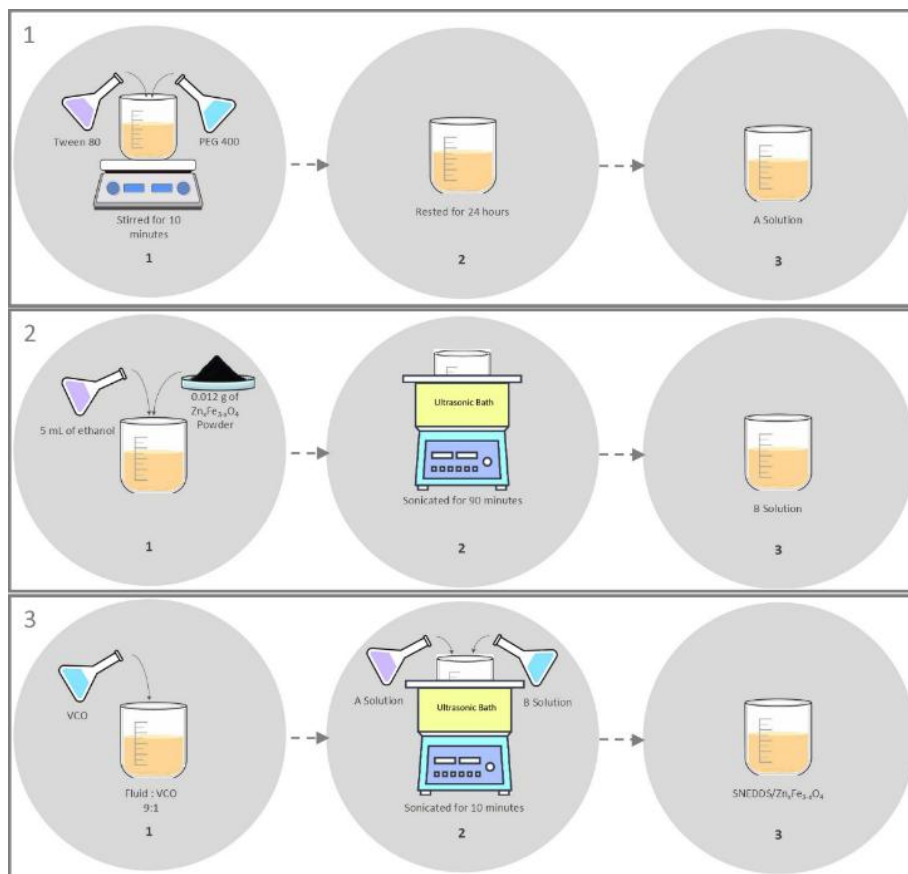| Sample Name	Sample Code
$SNEDDS/Fe_3O_4$	X0
$SNEDDS/Zn_{0.5}Fe_{2.5}O_4$	X1
$SNEDDS/ZnFe_2O_4$	X2
$SNEDDS/Zn_{1.5}Fe_{1.5}O_4$	X3

Figure 1. An illustration of the $SNEDDS/Zn_xFe_{3-x}O_4$ ferrofluid synthesis method

Characterizations

Characterization of $Zn_xFe_{3-x}O_4$ nanoparticles and $SNEDDS/Zn_xFe_{3-x}O_4$ ferrofluids was carried out using a Shimadzu brand Fourier Transform Infra-Red (FTIR) instrument to analyze the functional groups contained therein. X-ray Diffractometer (XRD) brand PANalytical with an angle of $10°-90°$ was used to determine the phase of the sample formed, particle size, and lattice parameters of $Zn_xFe_{3-x}O_4$ nanoparticles. XRD data were analyzed using Rietica with Fe_3O_4 model data. The antioxidant performance of $SNEDDS/Zn_xFe_{3-x}O_4$ ferrofluids used the DPPH method. The samples were characterized using the UV-Vis brand Analytic Jena. The samples characterizing antioxidant performance were measured as a solution inserted into a UV-Vis cuvette with the same volume of DPPH solution. The mixture was incubated at room

temperature for 30 to 60 minutes. Measure the absorbance of the reaction solution at the maximum wave number of DPPH (517 nm) using a UV-Vis spectrometer. Antioxidant performance analysis was carried out using *Excel* and *OriginLab* software. The percentage of antioxidant inhibition in the sample was calculated using a percentage. The calculation of IC_{50} to determine the antioxidant content was analyzed through the regression equation $y = ax-b$. Antioxidant compounds can be potent if the IC_{50} value reaches 50 ppm.

Results and Discussion

Functional Groups of $Zn_xFe_{3-x}O_4$ Nanoparticles

Figure 2 shows the results of FTIR characterization of $Zn_xFe_{3-x}O_4$ nanoparticles for samples X0, X1, X2, and X3. FTIR data analysis is presented in Table 3. Table 3 shows that O-H, C-O, C-H, Zn-O, and Fe-O functional groups represent bonds between atoms that make up the sample. Based on qualitative analysis, there is a change in the spectra's depth, indicating a change in absorption intensity in the sample [19][20]. The more molecules that absorb light at a specific wave number, the higher the absorption intensity value [21].
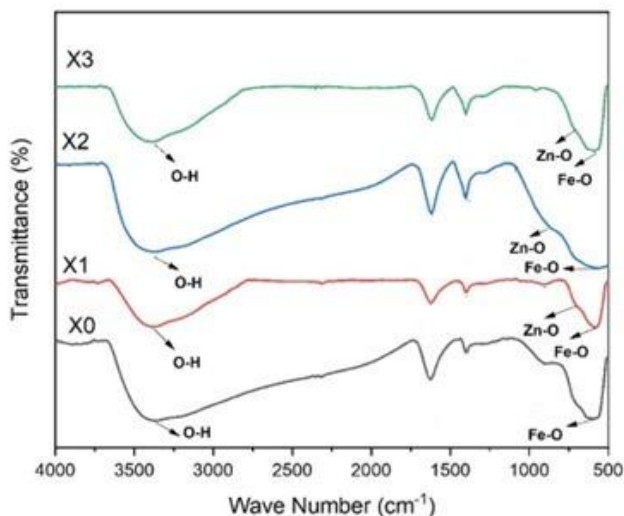

Figure 2. FTIR Spectra of X0, X1, X2, and X3 samples

The wave number range of 3700-3200 cm-1 indicates the O-H functional group detected at wave numbers 3375 cm-1, 3380 cm-1, 3378 cm-1, and 3410 cm-1 or samples X0, X1, X2, and X3, respectively. The absorption of the O-H functional group indicates the inclusion of H_2O in all samples due to the drying process not reaching optimal.

FTIR data analysis also shows the vibration of the C-O alcohol functional group in the 2000-1300 cm-1 range. This functional group was detected at wave numbers 1399 cm-1, 1399 cm-1, 1402 cm-1, and 1396 cm-1 for samples X0, X1, X2, and X3, respectively. In the low wave number area, the vibration of the sample was detected at wave numbers 594 cm-1, 580 cm-1, 560 cm-1, and 587 cm-1 for samples X0, X1, X2, and X3, respectively. These vibrations correspond to the wave number range of 600-450 cm-1, representing the Fe-O bond [22]. Meanwhile, for the wave number range of 900-800 cm-1, which is a representation of the Zn-O functional group bond, it

was detected only in 3 samples, namely samples X1, X2, and X3, each at wave numbers 823 cm^{-1}, 844 cm^{-1}, and 869 cm^{-1}. Thus, Zn doping was successfully carried out on $Zn_xFe_{3-x}O_4$ nanoparticles.

Table 3. Functional groups of X0, X1, X2, and X3 samples based on characterization using FTIR.

Functional Groups	Wavenumbers of Experiment Data (cm^{-1})				Wavenumbers of Previous Research (cm^{-1})
	X0	X1	X2	X3	
O-H	3375	3380	3378	3410	3700-3200 [22] [23]
Zn-O	-	823	844	869	900-800 [24][26]
Fe-O	594	580	560	587	600-450 [22] [25]

Crystal Structure of $Zn_xFe_{3-x}O_4$ Nanoparticles

The crystal structure of $Zn_xFe_{3-x}O_4$ nanoparticles was analyzed based on the XRD diffraction pattern. The XRD profiles of samples X0, X1, X2, and X3 are presented in Figure 3. The results of the XRD characterization were successfully analyzed using the Rietveld method with *Rietica* software. The analysis matched the Fe_3O_4 model data with the experimental XRD pattern. Based on the data analysis, the crystal structure of $Zn_xFe_{3-x}O_4$ is an inverse cubic spinel ($a = b = c$ and $a = \beta = \gamma$) occupying the *Fd3m* plane group. The lattice parameters of the sample showed an increase with the increasing Zn^{2+} doping composition on the $Zn_xFe_{3-x}O_4$ particles. In addition, the diffraction peak of the sample shifted towards a smaller 2θ angle with increasing Zn^{2+} doping composition. This confirms that Zn doping on $Zn_xFe_{3-x}O_4$ particles was successful, and the Zn^{2+} ions could shift the Fe3+ ions. The size of the Zn^{2+} and Fe^{3+} ions can explain this phenomenon. The Zn^{2+} ion has a diameter of 0.79 Å, more significant than the Fe^{3+} ion diameter of 0.64 Å [27]. The larger the doping diameter, the smaller the 2θ angle shift of the sample diffraction pattern.

This can be confirmed through the Bragg law equation. Based on Equation (2), when the lattice parameter (a) increases, the distance between the atoms (d) will increase. So, in Equation (3), when the distance between the atoms increases, the incoming diffraction angle (θ) will shift to a smaller angle. Thus, this theoretical study confirms that Zn^{2+} has been successfully substituted and replaced some of the Fe^{3+} atoms in $Zn_xFe_{3-x}O_4$ particles. The success of Zn^{2+} ions replacing Fe^{3+} ions, similar to the ionic radius and electron valence, impacts the peaks in the $Zn_xFe_{3-x}O_4$ XRD pattern, shifting towards a smaller angle. Details of the lattice parameters of samples X0, X1, X2, and X3 are shown in Table 4.

This can be confirmed through the Bragg law equation. Based on Equation (1), when the lattice parameter (a) increases, the distance between the atoms (d) will increase. So, in Equation (2), when the distance between the atoms increases, the incoming diffraction angle (θ) will shift to a smaller angle. Thus, this theoretical study confirms that Zn^{2+} has been successfully substituted and replaced some of the Fe^{3+} atoms in $Zn_xFe_{3-x}O_4$ particles. With the success of Zn^{2+} ions replacing Fe^{3+} ions as the similarity of ionic radius and electron valence, this has an impact on the peaks in the $Zn_xFe_{3-x}O_4$ XRD pattern shifting towards a smaller angle. Details of the lattice parameters of samples X0, X1, X2, and X3 are shown in Table 4.

$$d\ hkl = \frac{a}{\sqrt{h^2+k^2+l^2}} \tag{2}$$

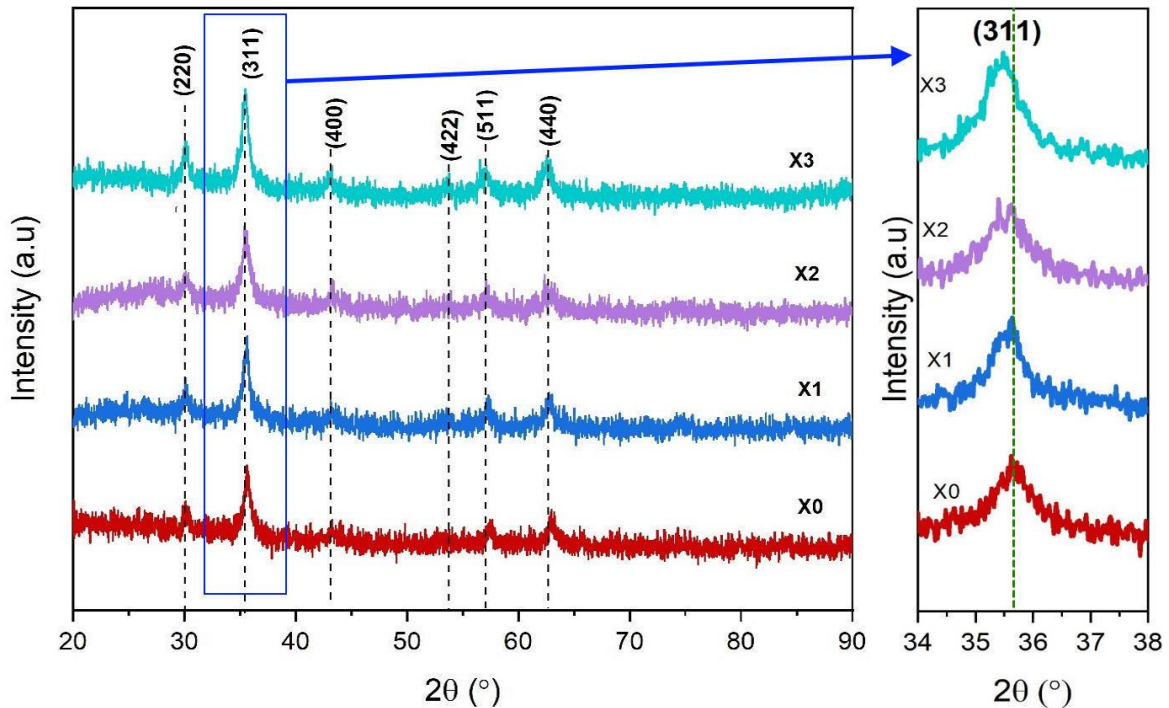$$n\lambda = 2d\sin\theta \qquad\qquad (3)$$

Figure 3. XRD pattern of X0, X1, X2, and X3 samples.

Table 4. Analysis result of XRD pattern of X0, X1, X2, and X3 samples,

Sample Code	Crystal Size (nm)	Rp	Rwp	χ^2	Bragg Factor	Lattice Parameter (a=b=c)
X0	12.30±0.020	5.09	6.33	1.13	3.49	8.3703±1.1x10⁻⁵
X1	11.70±0.019	4.94	6.25	1.04	3.24	8.3745±1x10⁻⁵
X2	11.20±0.120	5.14	6.51	1.08	2.82	8.3775±1.1x10⁻⁵
X3	9.93±0.029	5.27	6.66	1.11	3.51	8.3877±9x10⁻⁶

Parameters declared acceptable in XRD analysis using *Rietica* software are *Rp* and *Rwp*, which are less than 20%, *Bragg Factor* less than 10%, and the value of χ^2 less than 4%. Thus, the analysis output from refinement with Rietveld. Based on XRD data analysis, the greater the composition of Zn^{2+} doping, the more the crystallite size of the sample gradually decreases, as shown in Table 4. The decrease in crystallite size indicates that Zn^{2+} doping effectively replaces Fe^{3+} ions. This is in line with the research reported by Wang et al. [28]. The study showed that the more Zn^{2+} added, the smaller the crystallite size of the sample. In addition, the results of this study are supported by the research by Priyanka Saha et al. (2018), which stated that the diffraction peak shifted because Fe^{3+} was successfully replaced by Zn^{2+} [16]. Table 5 shows the shift of the diffraction peaks of the $Zn_xFe_{3-x}O_4$ material to a smaller angle by an average of 0.05. These results are in a line with the report by Wang et al. [28] and Anjana et al. [29], which showed a similar phenomenon, namely the shift of the particle diffraction peak towards a

smaller angle. Table 5 also shows how Zn^{2+} doping affects the lattice parameters of the sample. The larger the lattice parameter, the more significant the peak shift due to a Bragg plane in the XRD pattern, which will shift towards a smaller angle. This is according to Bragg's law, where the lattice parameter is inversely proportional to the change in angle [14] [15].

Table 5. Comparison of XRD peak for each Bragg Planes of X0, X1, X2, and X3 samples.

Sample Code	2θ (°)					
	(220)	(311)	(400)	(422)	(511)	(440)
X0	30.22	35.60	43.44	53.67	57.50	62.94
X1	30.18	35.52	43.32	53.55	57.33	62.72
X2	30.10	35.43	43.26	53.43	57.14	62.70
X3	30.06	35.45	43.17	53.40	67.02	62.56

Functional Groups of SNEDDS/$Zn_xFe_{3-x}O_4$ Ferrofluid

FTIR characterization was performed on SNEDDS X0, SNEDDS X1, SNEDDS X2, and SNEDDS X3 samples and presented in Figure 4. Based on Figure 4, the samples contain O-H, C=O, C=C, C-O, C-H, Zn-O, and Fe-O functional groups. The wave number range of 3371-3375 cm^{-1} indicates the O-H functional group representing the presence of alcohol in the SNEDDS sample [9] at a wave number of 3373 cm^{-1} for SNEDDS X0 and SNEDDS X1 samples and at wave numbers of 3375 and 3371 cm^{-1} for SNEDDS X2 and SNEDDS X3 samples, respectively. The vibration phenomenon at a wave number of 2862-2924 cm^{-1} indicates the presence of aliphatic C-H functional group bonds representing the presence of polymers and oils [30]. These results were confirmed in the wave number ranges of 2918-2862 cm^{-1}, 2922-2858 cm^{-1}, 2924-2868 cm^{-1}, 2920-2870 cm^{-1} for SNEDDS X0, SNEDDS X1, SNEDDS X2, and SNEDDS X3 samples, respectively. Vibrations were also detected in the wave number range of 1734-1737 cm^{-1}, indicating that the samples contain C=O functional groups corresponding to VCO and Tween 80 [31].

The results of FTIR data analysis also showed the detection of C=C bonds in the wave number range of 1643-1649 cm^{-1}, which confirmed the presence of antioxidant content [32]. Vibrations at wave numbers 1649 cm^{-1}, 1647 cm^{-1}, 1651 cm^{-1}, and 1643 cm^{-1}, which were respectively from samples SNEDDS X0, SNEDDS X1, SNEDDS X2, and SNEDDS X3, showed that all contained antioxidant materials. The 1251-1300 cm^{-1} wave number range indicated the C-O functional group [33]. This C-O functional group was detected at wave numbers 1109-1261 cm^{-1}, 1105-1288 cm^{-1}, 1112-1295 cm^{-1}, and 1114-1298 cm^{-1}, which were respectively representative of samples SNEDDS X0, SNEDDS X1, SNEDDS X2, and SNEDDS X3. The C-H vibration bonds at 650-1151 cm^{-1} [33] detected in this study for each sample of SNEDDS X0, SNEDDS X1, SNEDDS X2, and SNEDDS X3 are at 830-1049 cm^{-1}, 835-1095 cm^{-1}, 935-1095 cm^{-1}, and 833-1119 cm^{-1}. The wave number range of 833-848 cm^{-1} indicates the presence of Zn-O functional groups originating from the added Zn^{2+} doping [32]. The Zn-O functional group overlap with the C-H functional group. In this study, these were detected at 835 cm^{-1}, 948 cm^{-1}, and 833 cm^{-1} for each SNEDDS X1, SNEDDS X2, and SNEDDS X3 sample. Meanwhile, the 569-582 cm^{-1} wave number range indicates the Fe-O functional group [22]. The Fe-O functional group was detected well at wave numbers 569 cm^{-1}, 578 cm^{-1}, 503 cm^{-1}, and 572 cm^{-1} for SNEDDS X0, SNEDDS X1, SNEDDS X2, and SNEDDS X3 samples, respectively. All samples showed an

increasing absorption spectrum with increasing Zn concentration. This indicates that more compounds are absorbed in the wave number range [21]. The analysis results show a shift in the dominant peak to the left or towards a higher vibration frequency. This indicates that the chemical bonds in this peak are even more substantial. In detail, the functional groups and wave numbers of the SNEDDS/$Zn_xFe_{3-x}O_4$ Ferrofluid samples are presented in Table 6.
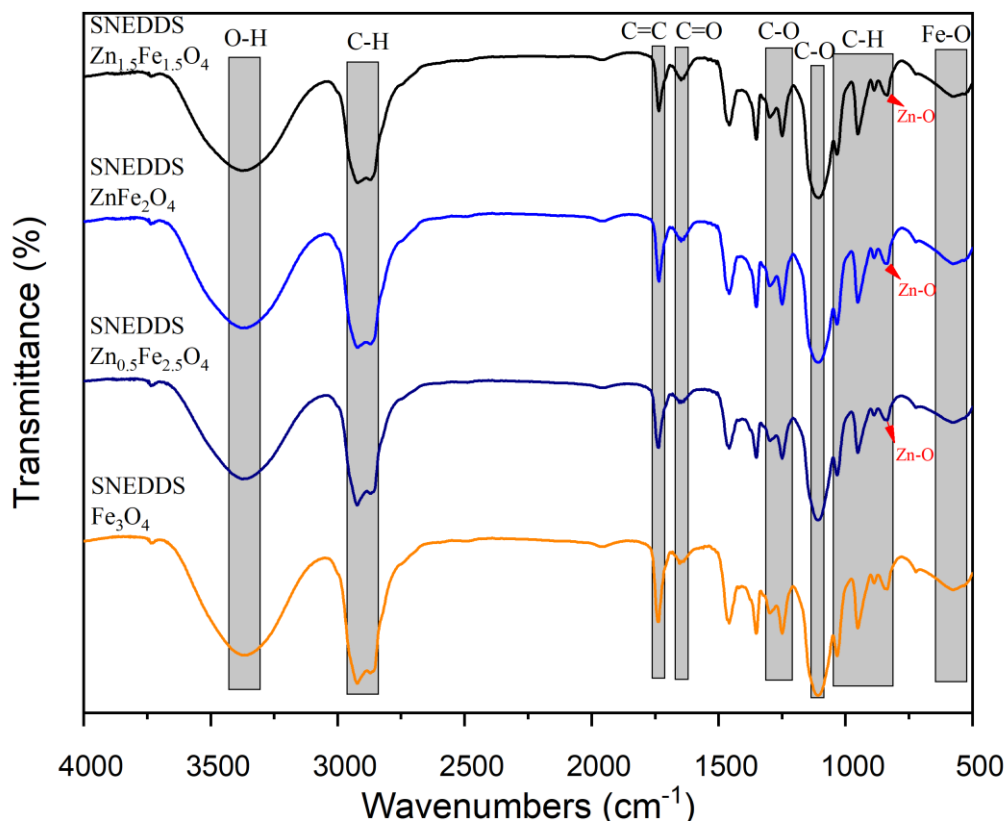

Figure 4. FTIR Spectra of SNEEDS X0, SNEDDS X1, SNEDDS X2, and SNEDDS X3 samples.

Antioxidant Performance of SNEDDS/$Zn_xFe_{3-x}O_4$ Ferrofluid

Characterization of antioxidant performance was carried out using the DPPH method. This test determined the antioxidant potential of the SNEEDS X0, SNEDDS X1, SNEDDS X2, and SNEDDS X3 samples. The results of the antioxidant test were in the form of the percentage of antioxidant inhibition of the sample. The percentage of antioxidant inhibition is the strength of the antioxidant in a sample [34]. The antioxidant results in the SNEEDS X0, SNEDDS X1, SNEDDS X2, and SNEDDS X3 samples can be seen in Table 7 and Figure 5. Based on the results of data analysis, the antioxidant inhibition of SNEDDS/$Zn_xFe_{3-x}O_4$ ferrofluid was in the range of 13% to 15%. SNEDDS/$Zn_xFe_{3-x}O_4$ ferrofluid's antioxidant inhibition increased with the Zn composition in the $Zn_xFe_{3-x}O_4$ nanoparticles. This shows that Zn can increase the antioxidant inhibition of the sample. Research reported by Ping Hou et al. 2022, showed that the antioxidant properties of Fe_3O_4 nanoparticles were 10% [17]. Compared with the results of

antioxidant tests on SNEEDS X0 or SNEDDS/Fe_3O_4, this study shows a higher antioxidant potential compared to previous research, namely 13%. Variations in the addition of Zn in other samples also showed higher antioxidants. This is due to the presence of Zn2+ doping and the influence of SNEDDS materials such as Tween 80, PEG 400, and VCO. Combining Zn^{2+}, Tween 80, PEG 400, and VCO doping can synergistically increase the antioxidant inhibition of SNEDDS/$Zn_xFe_{3-x}O_4$ ferrofluids. The Zn^{2+} oping can increase enzymatic activity, Tween 80 and PEG 400 can increase solubility and stability, while VCO can increase the overall antioxidant capacity.

Table 6. Functional groups of SNEDDS X0, SNEDDS X1, SNEDDS X2, and SNEDDS X3 samples based on characterization using FTIR

Functional Groups	Wavenumbers of Experiment Data (cm^{-1})				Wavenumbers of References (cm^{-1})
	X0	X1	X2	X3	
O-H	3373	3373	3375	3376	3710-3200 [9]
C-H	2918-2862	2922-2858	2924-2868	2920-2870	3150-2800 [30]
C=O	1735	1735	1737	1737	1750-1730 [31]
C=C	1649	1647	1651	1653	1680-1600 [32]
C-O	1109-1261	1105-1288	1112-1295	1114-1298	1300-1000 [32]
C-H	830-1049	835-1055	935-1095	833-1119	1151-650 [33]
Zn-O	-	835	935	833	900-800 [32]
Fe-O	569	572	573	573	696-559 [19]

Table 7. The result of antioxidant performance characterization to SNEDDS X0, SNEDDS X1, SNEDDS X2, and SNEDDS X3 samples using DPPH method.

Sample Code	Antioxidant Inhibition (%)
SNEDDS X0	13.60
SNEDDS X1	14.18
SNEDDS X2	14.62
SNEDDS X3	15.01

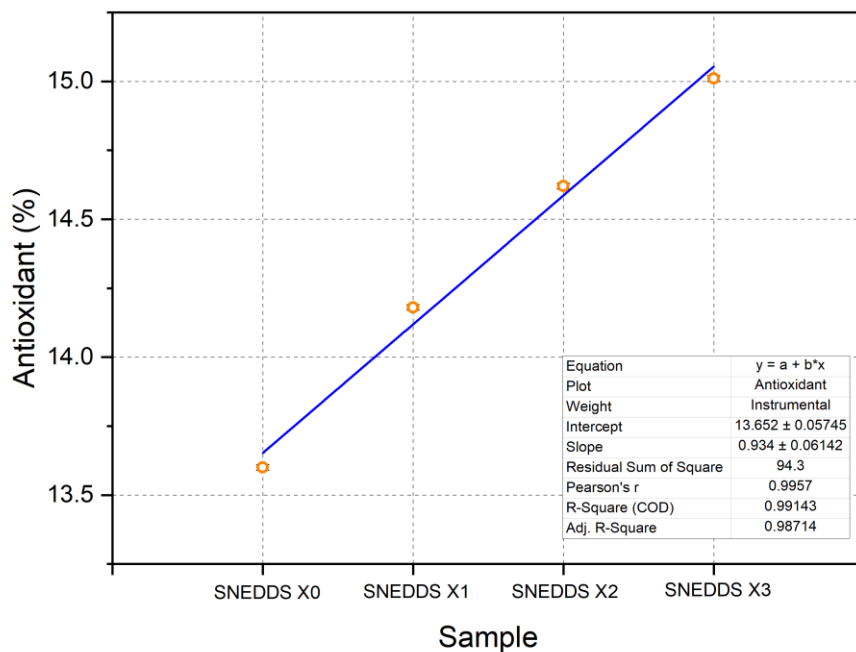| Equation	y = a + b*x
Plot	Antioxidant
Weight	Instrumental
Intercept	13.652 ± 0.05745
Slope	0.934 ± 0.06142
Residual Sum of Square	94.3
Pearson's r	0.9957
R-Square (COD)	0.99143
Adj. R-Square	0.98714

Figure 5. Percentage of antioxidant inhibitions of SNEDDS X0, SNEDDS X1, SNEDDS X2, and SNEDDS X3 samples.

Conclusion

Synthesis of $Zn_xFe_{3-x}O_4$ nanoparticles has been successfully carried out with variations in Zn composition with x of 0, 0.5, 1, and 1.5. The bonds of Fe-O and Zn-O functional groups were successfully detected at wave numbers 560-594 cm^{-1} and 825-869 cm^{-1}, respectively. Based on XRD data analysis, the crystal structure of $Zn_xFe_{3-x}O_4$ nanoparticles is a cubic spinel structure. The results of XRD data analysis also provide information that adding Zn^{2+} doping composition decreases particle size and shifts in the Bragg plane peak. The crystallite size of $Zn_xFe_{3-x}O_4$ nanoparticles gradually decreases from 12.30 nm to 9.93 nm, and the sample diffraction peak shifts towards a smaller angle as Zn^{2+} doping increases. When compared with previous research, Zn is effective in reducing particle size. This is because the diameter of the Zn^{2+} ion is much larger than that of the Fe^{3+} ion. The antioxidant inhibition of SNEDDS/$Zn_xFe_{3-x}O_4$ ferrofluid showed an increase from 13.6% to 15.01% with increasing Zn doping composition of $Zn_xFe_{3-x}O_4$ nanoparticles. The antioxidant yield of Fe_3O_4 nanoparticle powder was 10%, while for SNEDDS/Fe3O4 (SNEDDS X0), the experimental result was 13%. This shows that the ingredients for the SNEDDS formulation also contain antioxidants so that they can increase the antioxidant potential of SNEDDS/Fe_3O_4. Variations in adding Zn show that the antioxidant potential produced is more significant. This increase is a synergistic effect of SNEDDS/$Zn_xFe_{3-x}O_4$ ferrofluid components such as Zn^{2+} doping, Tween 80, PEG 400, and VCO.

Acknowledgment

References

[1] D. S. Prawitasari, "Diabetes Melitus dan Antioksidan," KELUWIH: Jurnal Kesehatan dan Kedokteran, vol. 1, no. 1, pp. 48–52, 2019.

[2] D. Prasonto, E. Riyanti, and M. Gartika, "Uji Aktivitas Antioksidan Ekstrak Bawang Putih (Allium sativum)," ODONTO : Dental Journal, vol. 4, no. 2, p. 122, 2017.

[3] J. Beno, A. P. Silen, and M. Yanti, "Covariance structure analysis of health-related indicators in elderly people living at home, focusing on subjective health status," Braz Dent J., vol. 33, no. 1, pp. 1–12, 2022.

[4] J. Patel, G. Kevin, A. Patel, M. Raval, and N. Sheth, "Design and development of a self-nanoemulsifying drug delivery system for telmisartan for oral drug delivery," International Journal of Pharmaceutical Investigation, vol. 1, no. 2, p. 112, 2017.

[5] N. Huda and I. Wahyuningsih, "Karakterisasi Self-Nanoemulsifying Drug Delivery System (SNEDDS) Minyak Buah Merah (Pandanus conoideus Lam.)," Jurnal Farmasi Dan Ilmu Kefarmasian Indonesia, vol. 3, no. 2, p. 49, 2018.

[6] A. A. Date, N. Desai, R. Dixit, and M. Nagarsenker, "Self-nanoemulsifying drug delivery systems: Formulation insights, applications and advances," Nanomedicine, vol. 5, no. 10, pp. 1595–1616, 2015.

[7] S. Priyani, " Pengaruh Pengembangan Self-Nanoemulsifying Drug Delivery System Terhadap Disolusi, Bioavailabilitas, Dan Aktivitas Agen Antihiperlipidemia," Jurnal Ilmiah Farmasi Farmasyifa, vol. 5, no. 1, pp. 101-111, 2022.

[8] M. Nadiah et al., "Preparation and Characterization of Self Nano-Emulsifying Drug Delivery System Loaded with Citraland Its Antiproliferative Effect on Colorectal Cells in Vitro," Nanomaterials, vol. 9, no. 1028, pp. 1–18, 2019.

[9] S. Prijic and G. Sersa, "Magnetic nanoparticles as targeted delivery systems in oncology," Radiology and Oncology, vol. 45, no. 1, pp. 1–16, 2018.

[10] I. O. Wulandari, "Pengembangan Metode Sintesis Nanopartikel Fe_3O_4 melalui Modifikasi Permukaan Berbasis Biokompatibel Molekul sebagai Kandidat Agen Drug Delivery," pp. 25–26, 2019.

[11] M. R. Ghazanfari, M. Kashefi, S. F. Shams, and M. R. Jaafari, "Perspective of Fe_3O_4 Nanoparticles Role in Biomedical Applications," Biochemistry Research International, vol. 2016, 2016.

[12] A. Astuti, I. Khaira, S. Arief, and S. R. A. Usna, "Sintesis dan Karakterisasi Struktur dan Sifat Magnet Nanokomposit Fe_3O_4@PEG:ZnO," Indonesian Journal of Applied Physics, vol. 12, no. 2, p. 217, 2022.

[13] Y. P. Yew et al., "Green biosynthesis of superparamagnetic magnetite Fe_3O_4 nanoparticles and biomedical applications in targeted anticancer drug delivery system: A review," Arabian Journal of Chemistry, vol. 13, no. 1, pp. 2287–2308, 2020.

[14] J. Sudimack and R. J. Lee, "Targeted drug delivery via the folate receptor," Advanced Drug Delivery Reviews, vol. 41, no. 2, pp. 147–162, 2018.

[15] L. B. Anigol, V. P. Sajjan, and P. M. Gurubasavaraj, "Evaluation of Antioxidant and Antibacterial Property of Microwave Assisted Green Synthesis of Fe_3O_4 -MgO Nanocomposites," IJST, vol. 16, no. 24, pp. 1777–1786, Jun. 2023.

[16] P. Saha, R. Rakshit, and K. Mandal, "Enhanced magnetic properties of Zn doped Fe_3O_4 nano hollow spheres for better bio-medical applications," Journal of Magnetism and Magnetic Materials, vol. 475, pp. 130–136, 2019.

[17] P. Hou, H. Kuang, W. Deng, and Y. Lei, "Immobilized copper nanoparticles on biodegradable magnetic starch composite: investigation of its ovarian cancer, cytotoxicity, and antioxidant effects," Journal of Experimental Nanoscience, vol. 17, no. 1, pp. 496–508, 2022.

[18] Usman, I. A. Fitri, and C. L. Suryani, "Pengaruh Jenis Medium Sumber Zn^{2+} dan Lama Blanching Terhadap Aktivitas Antioksidan Bubuk Simplisia Sambiloto (Andrographis Paniculata)," Prosiding Seminar Nasional Mini Riset Mahasiswa, vol. 1, no. 2, pp. 54–66, 2022.

[19] W. Setiani, T. Sudiarti, and L. Rahmidar, "Preparation and characterization of edible films from polunlend pati sukun-kitosan," Valensi, vol. 3, no. 2, pp. 100–109, 2015.

[20] Y. P. Utami, F. Maryam, S. Mus, and N. A. Agustin, "Fraksinasi dan Karakterisasi Senyawa Antioksidan Ekstrak Etanol Daun Andong Merah (Cordyline fruticosa (L.) A. Cheval) Menggunakan Uv-Vis dan FT-IR," Jurnal Mandala Pharmacon Indonesia, vol. 9, no. 2, pp. 273–281, 2023.

[21] I. Taufik and A. Aziz, "Degradasi Fotokatalitik Senyawa Metilen Biru Dengan Katalis Titania Nanotube," vol. 48, no. 283, pp. 53–60, 2024.

[22] P. Studi et al., "Formulasi SNEDDS Berbasis Partikel Nano Fe_3O_4 dengan Ekstrak Jahe (Zingiber officinale Roscoe) Sebagai Antioksidan," pp. 1–10, 2022.

[23] Y. K. Salimi, N. Bialangi, and S. Saiman, "Isolasi dan Identifikasi Senyawa Metabolit Sekunder Ekstrak Metanol Daun Kelor (Moringa oleifera Lamk.)," Akademika : Jurnal Ilmiah Media Publikasi Ilmu Pengetahuan dan Teknologi, vol. 6, no. 2, pp. 132–143, 2017.

[24] G. Gamah, K. Nastiti, and S. Aryzki, "Profil Senyawa Alkaloid Dengan Metode Spektroskopi Inframerah (FTIR) Dan Penetapan Kadar Total Alkaloid Dari Ekstrak Daun

Jarak Pagar (Jatropha curcas .L),” Journal Pharmaceutical Care and Sciences, vol. 4, no. 1, pp. 168–181, 2023.

[25] K. JASMINE, "Penambahan Natrium Benzoat Dan Kalium Sorbat (Antiinversi) Dan Kecepatan Pengadukan Sebagai Upaya Penghambatan Reaksi Inversi Pada Nira Tebu", vol. 9, no. 4, pp. 201–209, 2018.

[26] S. Bashir et al., “In-vivo (Albino Mice) and in-vitro Assimilation and Toxicity of Zinc Oxide Nanoparticles in Food Materials,” International Journal of Nanomedicine, vol. 17, no. September, pp. 4073–4085, 2022.

[27] L. Silvia, K. C. Rosyidah, and M. Zainuri, “Pengaruh Ion Doping Zn pada Sifat Kemagnetan Barium M-Heksaferit $BaFe_{12-x}Zn_xO_{19}$ berbasis Pasir Besi Tulungagung,” Jurnal Fisika dan Aplikasinya, vol. 9, no. 3, p. 121, 2013.

[28] X. Wang et al., “Adsorption of proteins on oral Zn^{2+} doped iron oxide nanoparticles in mouse stomach and: In vitro: Triggering nanoparticle aggregation,” Nanoscale, vol. 12, no. 44, pp. 22754–22767, 2020.

[29] P. M. Anjana, M. R. Bindhu, M. Umadevi, and R. B. Rakhi, “Antimicrobial, electrochemical and photo catalytic activities of Zn doped Fe_3O_4 nanoparticles,” Journal of Materials Science: Materials in Electronics, vol. 29, no. 7, pp. 6040–6050, 2018.

[30] V. A. Tiwow, M. J. Rampe, H. L. Rampe, and A. Apita, “Pola Inframerah Arang Tempurung Kelapa Hasil Pemurnian Menggunakan Asam,” Chemistry Progress, vol. 14, no. 2, p. 116, 2021.

[31] M. Sahu et al., “Fabrication of Cu_2ZnSnS_4 Light Absorber Using a Cost-Effective Mechanochemical Method for Photovoltaic Applications,” Materials, vol. 15, no. 5, pp. 1–16, 2022.

[32] I. O. Wulandari, L. B. Rahayu, I. Riva’i, H. Sulistyarti, and A. Sabarudin, “Sintesis dan Karakterisasi Nanopartikel Fe_3O_4 termodifikasi Biokompatibel Polimer serta Potensinya sebagai Penghantar Obat,” The Indonesian Green Technology Journal, pp. 1–8, 2021.

[33] A. Manohar, C. Krishnamoorthi, K. C. B. Naidu, and C. Pavithra, “Dielectric, magnetic hyperthermia, and photocatalytic properties of $ZnFe_2O_4$ nanoparticles synthesized by solvothermal reflux method,” Applied Physics A: Materials Science and Processing, vol. 125, no. 7, pp. 1–10, 2019.

[34] S. Widodo, N. Yusa, P. Timur Ina, " Pengaruh Waktu Maserasi Terhadap Aktivitas Antioksidan Ekstrak Daun Mundu (Garcinia dulcis (Roxb.) Kurz)," Jurnal Ilmu dan Teknologi Pangan (ITEPA), vol. 10, no. 5, pp. 14, 2021.